Monte Carlo simulation in the isobaric-multithermal ensemble of a bulk Lennard-Jones fluid system: Thermodynamic quantities for pressure from $P^*=2.42$ to 7.25

Chizuru Muguruma
School of Computational Science, Florida State University, Tallahassee, Florida 32306-4120, USA

Yuko Okamoto
Department of Physics, Nagoya University, Nagoya, Aichi 464-8602, Japan

(Received 31 August 2007; published 1 May 2008)

A Monte Carlo (MC) simulation in the isobaric-multithermal (MuTh) ensemble has been carried out for a bulk Lennard-Jones fluid system that consists of 108 particles. The MuTh weight factor which we determined turned out to be reliable for the temperature and pressure range from $(T^*,P^*)=(T_0^*,P_0^*)=(2.09,7.25)$ to $(T^*,P^*)=(0.417,1.45)$ along $P^*/T^*=P_0^*/T_0^*$. Thermodynamic quantities calculated from the MuTh MC production run by the reweighting techniques showed the discontinuous change, which is the feature of the first-order phase transition. The radial distribution functions suggest that the transition takes place between liquid and solid states. Two distinct local maxima were observed in the obtained contour representations of the probability distribution at $T^*=1.04$ and $P^*=3.63$, which is the phase transition point along $P^*/T^*=P_0^*/T_0^*$.

DOI: 10.1103/PhysRevE.77.051201 PACS number(s): 61.20.−p, 65.20.−w, 89.20.Ff, 82.60.Fa

I. INTRODUCTION

Conventional canonical simulations of complex systems with many degrees of freedom tend to get tapped at low temperatures in local minimum states on the potential energy surface. The multicanonical (MuCa) algorithm [1,2] has been introduced in order to overcome this multiple-minima problem and has been applied to study first-order phase transitions [1–16] (for recent reviews, see Refs. [17,18]). The algorithm is based on an artificial, non-Boltzmann weight factor and performs a free one-dimensional random walk in the potential energy space, which allows the simulation to avoid getting trapped in states of energy local minima. Moreover, one can calculate the expectation values of thermodynamic quantities as functions of temperature by applying the single-histogram reweighting techniques [19] to the results of one long production run. Hence, the MuCa ensemble can be considered to be the isochoric-multithermal ensemble.

The feature of the MuCa algorithm was recently extended into three generalized isobaric-isothermal algorithms, which are referred to as the multibaric-isothermal (MuBa), isobaric-multithermal (MuTh), and multibaric-multithermal (MuBaTh) algorithms [20,21]. These algorithms allow the simulations to escape from any states of energy local minima, and one can obtain various isobaric-isothermal ensembles and calculate the expectation values of thermodynamic quantities as functions of any temperature and pressure by applying the reweighting techniques to the results of one long production run. The MuBa Monte Carlo (MC) simulation performs a random walk in the volume space under the given temperature T_0. The MuTh MC simulation performs a random walk in the potential energy space along the line $P/T=P_0/T_0$, where P_0 is the given pressure. The MuBaTh MC simulation performs a random walk in both potential energy space and volume space. Therefore, the reweighting techniques are employed in the restricted temperature T_0 for the MuBa ensemble, and in the restricted pressure-temperature ratio $P/T=P_0/T_0$ for the MuTh ensemble, while there is no restriction for pressure and temperature for the MuBaTh ensemble. The most outstanding feature of these generalized-ensemble algorithms lies in the following fact. While one cannot see two distinct configurational phases coexisting in the same simulation for the conventional molecular simulation method at constant pressure and temperature [22], these new algorithms allow the simulation to visit both phases across the phase transition point many times within a single run. Hence, one can study the transition states of phase transition in detail.

A Lennard-Jones fluid system is one of typical systems with first-order phase transitions [7,10,15,16,20,21,23–31]. In previous works, we have investigated the phase transition of the argon (Lennard-Jones) fluid by using the MuCa MC method [15,16]. One of the problems of this method was that the pressure of the system changed from 0.61 GPa ($P^*=14.6$) to zero as temperature varied from 250 K ($T^*=2.09$) to 50 K ($T^*=0.417$) because the number of particles and volume were fixed in the MuCa ensemble. The transition temperature was 148 K ($T^*=1.24$) at 0.30 Gpa ($P^*=7.25$) [15]. Besides, most of the experimental data are obtained under constant pressure, especially under 1 atm. In the present study, we investigated the liquid-solid phase transition under constant pressure. We applied the MuTh MC method [20] to the bulk Lennard-Jones system and investigated the changes in thermodynamic quantities across the phase transition point from $P^*=2.42$ to 7.25.

This paper is organized as follows. In Sec. II, the MuTh MC method is briefly described. We report the results of the MuTh MC simulation of a Lennard-Jones system in Sec. III. Conclusions follow in Sec. IV.

II. COMPUTATIONAL METHODS

Although the MuTh algorithm, which is an extension of multicanonical algorithm to the isobaric-multithermal ensemble, is explained elsewhere [20], we give a short overview in this section for completeness.

A. Canonical and *N-P-T* MC simulations

In the canonical (conventional *N-V-T*) ensemble, the probability distribution $P_B(E;T_0)$ of the potential energy E under temperature T_0 is given by the product of the density of states $n(E)$ and the Boltzmann weight factor $w_B(E;T_0)$,

$$P_B(E;T_0) \propto n(E)w_B(E;T_0) = n(E,V)\exp(-\beta_0 E), \quad (1)$$

where β_0 is the inverse temperature $1/k_B T_0$ with the Boltzmann constant k_B and temperature T_0 and $P_B(E;T_0,)dE$ is the probability of finding the system in interval E and $E+dE$. Because $n(E)$ is a rapidly increasing function and $w_B(E;T_0)$ decreases exponentially, $P_B(E;T_0)$ generally has a bell-like shape.

Here, we consider a system that consists of N particles with total potential energy E. A conventional MC simulation is performed with the usual Metropolis criterion [32]. In the canonical MC simulation, the transition probability of state x with potential energy E to state x' with potential energy E' is given by

$$w(x \to x') = \begin{cases} 1, & \text{for } \Delta W_{NVT} \le 0, \\ \exp(-\Delta W_{NVT}), & \text{for } \Delta W_{NVT} > 0, \end{cases} \quad (2)$$

where $\Delta W_{NVT} \equiv \beta(E'-E)$.

In the conventional *N-P-T* ensemble, the probability distribution $P_{NPT}(E,V;T_0,P_0)$ of the potential energy E and volume V under pressure P_0 and temperature T_0 is given by the product of the density of states $n(E,V)$ and the *N-P-T* weight factor $w_{NPT}(E,V;T_0,P_0)$:

$$P_{NPT}(E,V;T_0,P_0) \propto n(E,V)w_{NPT}(E,V;T_0,P_0) = n(E,V)\exp[-\beta_0(E+P_0V)], \quad (3)$$

where the *N-P-T* weight factor is the product of the Boltzmann weight factor and $\exp(-\beta_0 P_0 V)$. Since $n(E,V)$ is a rapidly increasing function and $w_{NPT}(E,V;T_0,P_0)$ decreases exponentially, $P_{NPT}(E,V;T_0,P_0)$ generally has also a bell-like shape in the *E-V* space. In the MC simulation in the *N-P-T* ensemble, the transition probability of state x with potential energy E and volume V to state x' with potential energy E' and volume V' is given by

$$w(x \to x') = \begin{cases} 1 & \text{for } \Delta W_{NPT} \le 0, \\ \exp(-\Delta W_{NPT}) & \text{for } \Delta W_{NPT} > 0, \end{cases} \quad (4)$$

where

$$\Delta W_{NPT} \equiv \beta(E'-E) + \beta_0 P_0 (V'-V) - N \ln\left(\frac{V'}{V}\right). \quad (5)$$

The conventional MC simulation is carried out by generating a Markov chain of states which follows the ensemble. Thus, the expectation value of a physical quantity θ is given by

$$\langle\theta\rangle = \frac{1}{N_S}\sum_{k=1}^{N_S} \theta^{(k)}, \quad (6)$$

where N_S is the total number of the samples and $\theta^{(k)}$ is θ at the kth sample.

B. MuTh MC simulations

In the MuTh ensemble, each state is weighted by an artificial, non-Boltzmann weight factor $w_{\mathrm{MuTh}}(E)$, which we refer to as the MuTh weight factor, so that a uniform potential energy distribution may be obtained under the constant pressure P_0,

$$\int dV P_{\mathrm{MuTh}}(E,V;P_0) \propto \int dV n(E,V)\exp(-\beta_0 P_0 V) w_{\mathrm{MuTh}}(E) \equiv n_{\mathrm{MuTh}}(E) w_{\mathrm{MuTh}}(E) \equiv \text{const}, \quad (7)$$

where we denote $\int dV n(E,V)\exp(-\beta_0 P_0 V)$ as $n_{\mathrm{MuTh}}(E)$ and we can treat $n_{\mathrm{MuTh}}(E)$ of the MuTh ensemble like $n(E)$ of the multicanonical ensemble. The flat artificial energy distribution implies that a one-dimensional free random walk in the potential energy space is realized. The random walk allows the system to escape from any local-minimum-energy states and to sample the configurational space much more widely with a smaller number of simulation steps than the conventional MC or molecular dynamics methods.

According to the definition in Eq. (7), the MuTh weight factor $w_{\mathrm{MuTh}}(E)$ is inversely proportional to $\int dV n(E,V)\exp(-\beta_0 P_0 V)$ and can be written as follows:

$$w_{\mathrm{MuTh}}(E) \equiv \exp\left(-\frac{S_{\mathrm{mic}}(E)}{k_B}\right) = \frac{1}{\int dV n(E,V)\exp(-\beta_0 P_0 V)} \equiv \frac{1}{n_{\mathrm{MuTh}}(E)}, \quad (8)$$

where $S_{\mathrm{mic}}(E)$ is the entropy in the microcanonical ensemble,

$$S_{\mathrm{mic}}(E) = k_B \ln \int dV n(E,V)\exp(-\beta_0 P_0 V) \equiv k_B \ln n_{\mathrm{MuTh}}(E), \quad (9)$$

and we can write the inverse temperature $\beta(=1/k_B T)$ as follows:

$$\beta = \frac{1}{k_B}\frac{dS_{\mathrm{mic}}(E)}{dE}. \quad (10)$$

The relation between $S_{\mathrm{mic}}(E)$ in Eqs. (8) and (9) and $E_{\mathrm{mt}}(E)$ in Eq. (30) of Ref. [20] for the MuTh algorithm is $S_{\mathrm{mic}}(E)/k_B = \beta_0 E_{\mathrm{mt}}(E)$. Since the density of states $n_{\mathrm{MuTh}}(E)$ of the system is usually unknown, the MuTh weight factor must be determined numerically by iterations of short preliminary runs. In the present study, we employed the iterative procedure in Ref. [33] as well as the single-histogram [19] and multiple-histogram [34,35] reweighting techniques.

A MuTh MC simulation is also performed with the usual Metropolis criterion [32]: The transition probability of state x with potential energy E and volume V to state x' with potential energy E' and volume V' is given by

$$w(x \to x') = \begin{cases} 1 & \text{for } \Delta W_{\mathrm{MuTh}} \le 0, \\ \exp(-\Delta W_{\mathrm{MuTh}}) & \text{for } \Delta W_{\mathrm{MuTh}} > 0, \end{cases} \quad (11)$$

where

$$\Delta W_{\mathrm{MuTh}} \equiv \frac{S_{\mathrm{mic}}(E') - S_{\mathrm{mic}}(E)}{k_B} + \beta_0 P_0 (V' - V) - N \ln\left(\frac{V'}{V}\right). \tag{12}$$

Note that $\beta(E'-E)$ in Eq. (5) for the N-P-T ensemble changes into $S_{\mathrm{mic}}(E')-S_{\mathrm{mic}}(E)/k_B$ in the MuTh ensemble.

Once the MuTh weight factor [equivalently the entropy $S_{\mathrm{mic}}(E)$] is determined, one performs a long MuTh production run. By tracing the potential energy surface during the simulation, the global-minimum energy state can be identified. Moreover, adopting the reweighting techniques, the probability distribution $P_{NPT}(E,V;T,P)$ and the expectation value of a physical quantity θ at any temperature $T(=1/k_B\beta)$ and pressure P are given by [see Eq. (7)]

$$\begin{aligned} P_{NPT}(E,V;T,P) &\propto n(E,V)\exp[-\beta(E+PV)] \\ &= H_{\mathrm{MuTh}}(E,V;P_0) w^{-1}_{\mathrm{MuTh}}(E)\exp(\beta_0 P_0 V) \\ &\quad \times \exp[-\beta(E+PV)] \end{aligned} \tag{13}$$

and

$$\langle \theta \rangle_{NPT} = \frac{\int dE \int dV \theta(E,V) P_{NPT}(E,V;T,P)}{\int dE \int dV P_{NPT}(E,V;T,P)}, \tag{14}$$

respectively, where $H_{\mathrm{MuTh}}(E,V;P_0)$ is the histogram of the distribution of E and V obtained for the MuTh production run.

C. Computational details

We set 108 particles in a cubic cell with periodic boundary conditions. A pair of particles with distance r_{ij} interact through the Lennard-Jones pair potential

$$v(r_{ij}) = 4\varepsilon\left[\left(\frac{\sigma}{r_{ij}}\right)^{12} - \left(\frac{\sigma}{r_{ij}}\right)^{6}\right]. \tag{15}$$

Hereafter, the length and energy are scaled in units of Lennard-Jones diameter σ and the depth of the potential ε, respectively. We use an asterisk for the reduced quantities such as the reduced distance $r^*=r/\sigma$, the reduced energy $E^*=E/\varepsilon$, the reduced volume $V^*=V/\sigma^3$, the reduced pressure $P^*=P\sigma^3/\varepsilon$, the reduced temperature $T^*=k_BT/\varepsilon$, and the reduced number density $\rho^*=\rho/\sigma^3$.

The total potential energy of the system that consists of N particles is given by

$$E^* = \sum_{i=1}^{N-1} \sum_{j>i}^{N} v^*(r_{ij}^*), \tag{16}$$

where the interactions of all particles are truncated at one-half of a length of the edge size $r_c(=L/2)$ and the potential energy is corrected by the following equation:

$$E_N^{c*} = \frac{8}{9}\pi N \rho^* \left[\left(\frac{1}{r_c^*}\right)^9 - 3\left(\frac{1}{r_c^*}\right)^3\right]. \tag{17}$$

The MuTh weight factor was determined for the energy range below $E^*=-4.78$ that corresponds to the temperature range $T^* \leq 2.09$ under the initial pressure of $P^*=7.25$. Thermodynamic quantities were calculated by the reweighting techniques in Eqs. (13) and (14). For instance, heat capacity C_P was calculated from the following equation:

$$C_P^* = \frac{\langle H^{*2}\rangle_{NPT} - \langle H^*\rangle^2_{NPT}}{T^{*2}}, \tag{18}$$

where the enthalpy H^* is given by $H^*=E^*+P^*V^*$ and the given pressure in the reweighting formula P^* is used as pressure for the calculation.

Applying the reweighting formulas in Eqs. (13) and (14), the pressure in the N-P-T ensemble is also estimated at any temperature T^* and pressure P^* by the following equation:

$$\langle P^* \rangle_{NPT} = \frac{\int dE^* \int dV^* P^*_{\mathrm{temp}}(E^*,V^*) P_{\mathrm{MuTh}}(E^*,V^*;P^*_{0*}) w^{-1}_{\mathrm{MuTh}}(E^*)\exp(\beta_0^* P_0^* V^*)\exp[-\beta^*(E^*+P^*V^*)]}{\int dE^* \int dV^* P_{\mathrm{MuTh}}(E^*,V^*;P_0^*) w^{-1}_{\mathrm{MuTh}}(E^*)\exp(\beta_0^* P_0^* V^*)\exp[-\beta^*(E^*+P^*V^*)]}, \tag{19}$$

where

$$P^*_{\mathrm{temp}}(E^*,V^*) = P^*_{\mathrm{ins}} + P^{c*} \tag{20}$$

as $\theta^*(E^*,V^*)$ in Eq. (14). Here, the instantaneous pressure P^*_{ins} is given by

$$P^*_{\mathrm{ins}} = \frac{NT^*}{V^*_{\mathrm{ins}}} + \frac{1}{3V^*_{\mathrm{ins}}} \sum_{i=1}^{N-1} \sum_{j>i}^{N} r^*_{ij} f^*_{ij}, \tag{21}$$

where f^*_{ij} is the pair force acting on atom i due to atom j, V^*_{ins} is the instantaneous volume of the system, and T^* is the temperature that is obtained from Eq. (10). The contribution of the particles beyond the truncation at r_c in pressure is corrected by the following equation:

$$P^{c*} = \frac{16}{9}\pi \rho^{*2} \left[2\left(\frac{1}{r_c^*}\right)^9 - 3\left(\frac{1}{r_c^*}\right)^3\right]. \tag{22}$$

To investigate the change in pressure of the system during the MuTh MC simulation, the average pressure is also calculated with the MuTh weight factor $w_{\mathrm{MuTh}}(E^*)$ by the following equation:

$$\langle P^* \rangle_{\text{therm}} = \frac{\int dE^* \int dV^* P^*_{\text{temp}}(E^*,V^*) P_{\text{MuTh}}(E^*,V^*;P^*_0) w^{-1}_{\text{MuTh}}(E^*) \exp(-\beta^* E^*)}{\int dE^* \int dV^* P_{\text{MuTh}}(E^*,V^*;P^*_0) w^{-1}_{\text{MuTh}}(E^*) \exp(-\beta^* E^*)}. \tag{23}$$

Here, Eq. (23) becomes exactly the same equation as the reweighting techniques for pressure in the *N-P-T* ensemble in Eq. (19) when $P^*/T^* = P^*_0/T^*_0$.

Calculating free energy and entropy by the ordinary molecular simulation methods requires a lot of effort. In the MuTh ensemble, the Gibbs free energy G^* at temperature $T^*(=\beta^{*-1})$ and pressure P^* is obtained by the following equation:

$$G^*(T^*,P^*) = -\beta^{*-1} \ln Z, \tag{24}$$

where Z is the partition function and is expressed as

$$Z = \int dE^* \int dV^* n(E^*,V^*) \exp[-\beta^*(E^* + P^* V^*)] = \int dE^* \int dV^* P_{\text{MuTh}}(E^*,V^*;P^*_0) w^{-1}_{\text{MuTh}}(E^*) \exp(\beta^*_0 P^*_0 V^*) \exp[-\beta^*(E^* + P^* V^*)] \tag{25}$$

in the MuTh algorithm. We remark that the conventional *N-P-T* ensemble simulation cannot give accurate free energy G for Eq. (24) for low T^* and high P^*, because the simulation will get trapped in states of local minima. Entropy is also one of the physical quantities that are difficult to calculate by the ordinary computer simulation methods. The entropy in the *N-P-T* ensemble at temperature T^* and pressure P^* is simply calculated by the relation $G^* = H^* - T^* S^*$:

$$S^*(T^*,P^*) = -\frac{G^*(T^*,P^*) - H^*(T^*,P^*)}{T^*}, \tag{26}$$

where $H^*(T^*,P^*) = \langle H^* \rangle_{NPT}$, and the reweighting formulas in Eqs. (13) and (14) were used with $\theta = H^*$.

One MC sweep is defined to consist of 108 coordinate updates of a randomly chosen particle and a random volume change with the Metropolis evaluation for each update. All calculations were performed with our own computer code.

III. RESULTS AND DISCUSSION

A. MuTh weight factor

Figure 1 shows the best estimate of the microcanonical entropy $S^*_{\text{mic}}(E^*)$ that is related to the MuTh weight factor as in Eq. (8). The entropy shows a depression in its curvature around $E^* = -6.55$ which is the border between two phases. The "time series" of total potential energy from the MuTh MC production run is shown in Fig. 2(a). We indeed see a random walk between $E^* = -8.02$ and -4.78. The energy region is divided into two parts around $E^* = -6.55$, and the significant transitions between these two regions took place at least 10 times during the MuTh MC production run.

The MuTh MC simulation is equivalent to a parallel run of conventional *N-P-T* ensembles at many (T^*,P^*)'s. As we describe in Sec. III C, the potential energy fluctuates in the potential energy and volume space along $P^*/T^* = P^*_0/T^*_0$ with $P^*_0 = 7.25$ and $T^*_0 = 2.09$. To demonstrate the temperature and pressure range of the present MuTh MC simulation, the "time series" of total potential energy obtained by the conventional MC simulations for the conventional *N-P-T* ensemble with 5×10^7 MC sweeps at $(T^*,P^*) = (0.417, 1.45)$ and $(T^*,P^*) = (2.09, 7.25)$ are shown in Fig. 2(b). The potential energies fluctuate in the potential energy and volume space under the restriction of (T^*,P^*) and ensemble averages of (T^*,P^*) must be (2.09, 7.25), and (0.417, 1.45), respectively. Comparing the energy regions covered between Figs. 2(a) and 2(b), the MuTh MC production run covered a wide temperature and pressure range, which is from $(T^*,P^*) = (0.417, 1.45)$ to $(T^*,P^*) = (2.09, 7.25)$ in the vicinity of the line $P^*/T^* = P^*_0/T^*_0$.

The histogram that was obtained by the MuTh MC production run is shown in Fig. 3. Because the histogram is directly proportional to $\int dV P_{\text{MuTh}}(E,V;P_0)$ in Eq. (7), it is ideally uniform. We observe a flat histogram in the energy regions between $E^* = -8.02$ and -6.58 and between $E^* = -6.50$ and -4.80, while we can see a kink around $E^* = -6.55$. This kink is apparently caused by infrequent transitions between higher and lower energy regions. The magnitude of the histogram at the higher energy region is at least of the same order as that at the lower energy region. We conclude that the MuTh ensemble is realized in the energy region between $E^* = -8.02$ and -4.80.

B. Thermodynamic quantities

Some thermodynamic quantities were calculated as the expectation values of physical quantities at every $T^* = 4.17 \times 10^{-2}$ from 0.417 to 2.09 for $P^* = 2.42$, 3.63, 4.84, 6.05, and 7.25. Average volume, enthalpy, entropy, Gibbs free energy, and heat capacity are shown in Fig. 4. These were obtained by the MuTh MC production run by the reweighting techniques in Eqs. (13) and (14). We can observe the discontinuous change for average volume, enthalpy, and entropy, the change in the slope for Gibbs free energy, and a significant peak for heat capacity. These "discontinuities" are the characteristics of the first-order phase transitions and are at T^*

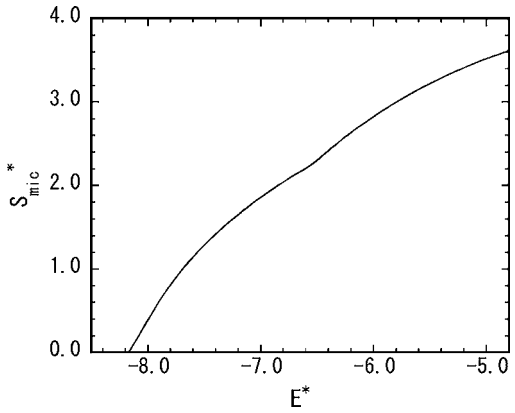

FIG. 1. Entropy as a function of total potential energy obtained by the MuTh MC production run. We have set the value of entropy to zero at $E^*=-8.17$.

$=T_c^*=1.29$ for $P^*=7.25$, at $T_c^*=1.21$ for $P^*=6.05$, at $T_c^*=1.13$ for $P^*=4.84$, at $T_c^*=1.04$ for $P^*=3.63$, and at $T_c^*=0.943$ for $P^*=2.42$. The transition temperature $T_c^*=1.29$ for $P^*=7.25$ agrees well with $T_c^*=1.24$ for $P^*=7.25$ of the MuCa simulation [15]. These values of (T_c^*,P^*) are on the melting line obtained from the simulation of the Lennard-Jones fluids [24,26].

The discontinuities in enthalpy at the phase transition point are $\Delta H_c^*=1.7$ for $P^*=7.25$, $\Delta H_c^*=1.6$ for $P^*=6.05$, $\Delta H_c^*=1.5$ for $P^*=4.84$, $\Delta H_c^*=1.4$ for $P^*=3.63$, and $\Delta H_c^*=1.3$ for $P^*=2.42$, which agrees well with the thermodynamic enthalpy $\Delta H_m=1.142$ at melting point $(T_m,P_m)=(0.780,0.947)$ for the Lennard-Jones system [36]. The discontinuities in volume are approximately $\Delta V_c^*\approx 0.1$ at every transition temperature for every given pressure. The average volume changes from $V^*=0.98$ to $V^*=1.09$ at $T_c^*=1.13$ for $P^*=4.84$, which agrees well with the change in the number density of the Lennard-Jones fluid from $\rho^*=1.02$ $(V^*=0.98)$ of solid state to $\rho^*=0.938$ $(V^*=1.07)$ of liquid state at $T_c^*=1.15$ and $P^*=5.68$ [37]. The discontinuity in entropy is approximately $\Delta S_c^*=1.3$ at every transition temperature for every given pressure, which agrees well with the thermodynamic entropy $\Delta S_m=1.46$ at melting point $(T_m,P_m)=(0.780,0.947)$ for the Lennard-Jones system [36,38]. Besides, the difference in isochoric entropy between crystalline and noncrystalline states of Lennard-Jones fluid was $\Delta S_c^*=0.6$ [39], the discontinuity in isochoric entropy was $\Delta S_c^*=0.57$ in the MuCa simulation [15], and the discontinuity in the microcanonical entropy was $\Delta S_{\mathrm{mic},c}^*=0.85$ at $(T^*,P^*)=(1.23,7.25)$ in the present simulation. We remark that the differences in enthalpy and in entropy at the phase transition point satisfy the thermodynamic relation $\Delta S_c^*=\Delta H_c^*/T_c^*$.

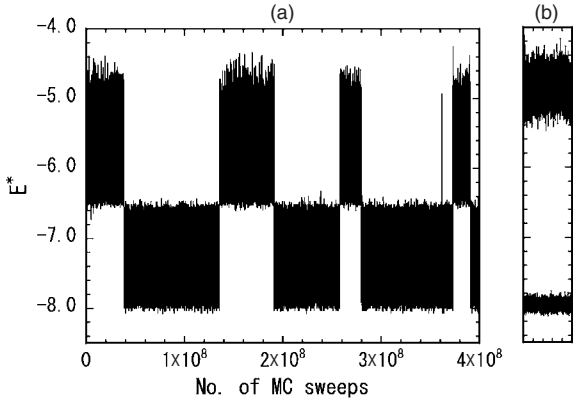

FIG. 2. Time series of total potential energy obtained by (a) a long production run of the MuTh MC simulation and (b) the conventional Monte Carlo calculations for N-P-T ensemble at $(T^*,P^*)=(0.417,1.45)$ and $(T^*,P^*)=(2.09,7.25)$. In (b), the upper curve corresponds to $(T^*,P^*)=(2.09,7.25)$, while the lower curve corresponds to $(T^*,P^*)=(0.417,1.45)$.

The slope of the phase boundary for melting (fusion) is obtained from the Clapeyron equation

$$\frac{dP}{dT}=\frac{\Delta_{\mathrm{fus}}H}{T\Delta_{\mathrm{fus}}V}. \tag{27}$$

Therefore, the approximate equation of the solid-liquid boundary becomes

$$P\approx P'+\frac{(T-T')\Delta_{\mathrm{fus}}H}{T'\Delta_{\mathrm{fus}}V}, \tag{28}$$

when T is close to T'. By substituting $\Delta_{\mathrm{fus}}H=\Delta H_c^*=1.4$ and $\Delta_{\mathrm{fus}}V=\Delta V_c^*\approx 0.10$ at $T'=T_c^*=1.04$ for $P'=P^*=3.63$, the equation becomes

$$P^*\approx 14T_c^*-10. \tag{29}$$

This equation agrees well with the least-squares fit of the melting temperatures under the given pressure P^*,

$$P^*=13.9T_c^*-10.8, \tag{30}$$

which was obtained by the linear fitting in Fig. 6 below.

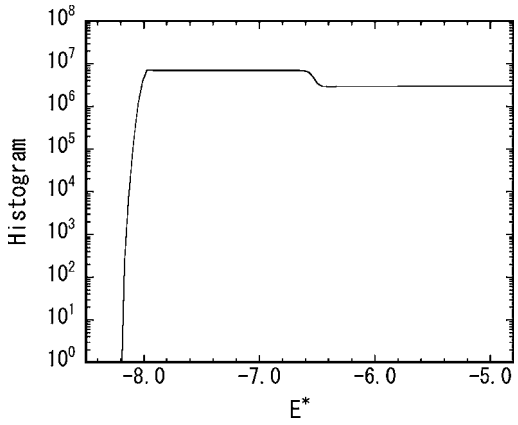

FIG. 3. Histogram of the total potential energy distribution that was obtained by the MuTh MC production run.

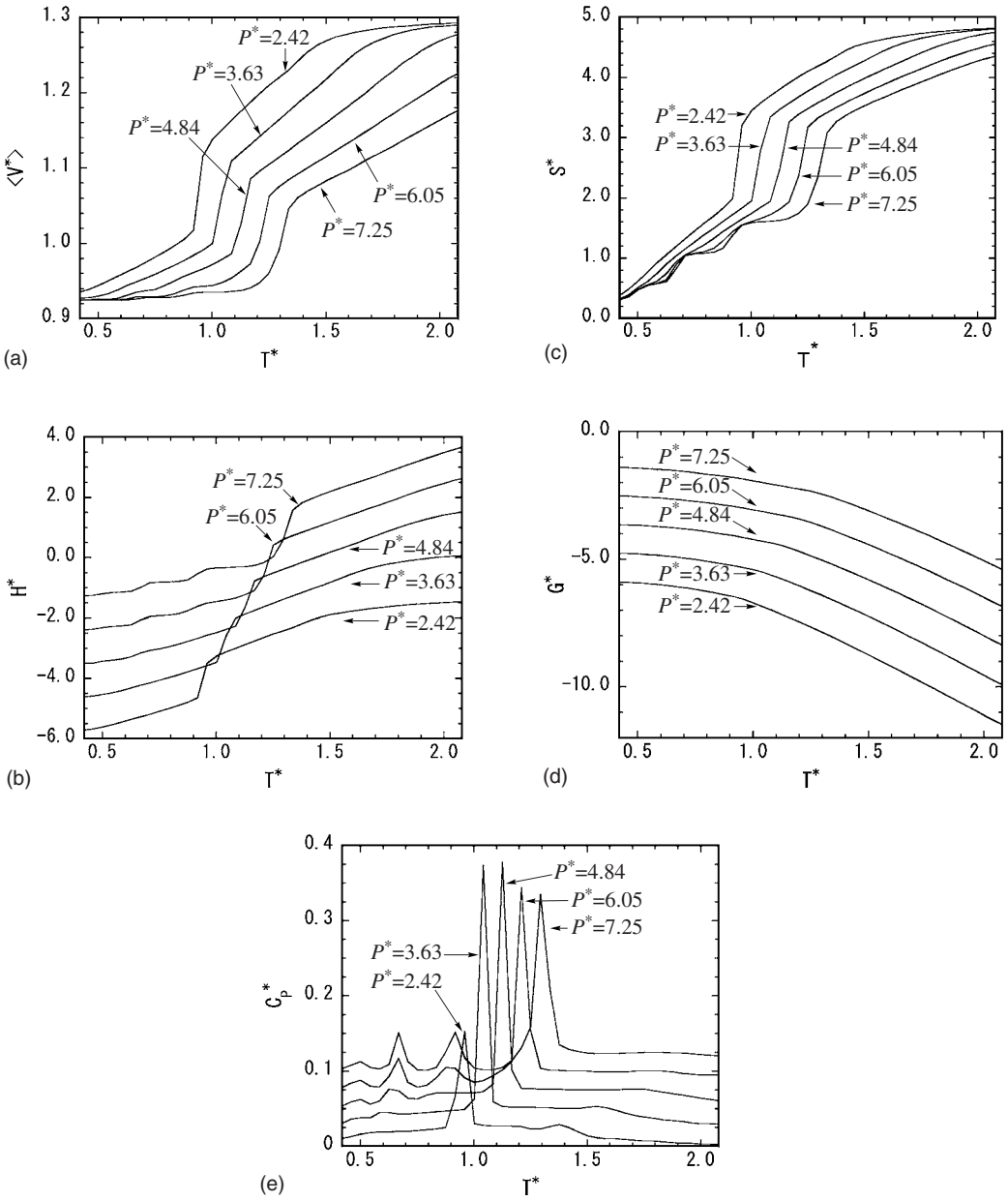

FIG. 4. Thermodynamic quantities obtained from the MuTh MC production run by the reweighting techniques for (a) average volume, (b) enthalpy, (c) entropy, (d) Gibbs free energy, and (e) heat capacity. The expectation values were calculated for $P^*=2.42$, 3.63, 4.84, 6.05, and 7.25 at each $T^*=4.17\times10^{-2}$ from 0.417 to 2.09. Heat capacities are shifted by 0.25 as pressure rises by $P^*=1.21$ from 2.42 to 7.25.

Concerned with the relations among temperature, enthalpy and Gibbs free energy under the given pressure P^*, we confirmed that the Gibbs-Helmholtz equation is satisfied (data not shown),

$$\frac{\partial}{\partial\left(\frac{1}{T^*}\right)}\left(\frac{G^*}{T^*}\right)=H^*. \tag{31}$$

Gibbs free energy increases $\Delta G^*\approx1.1$ at any temperature as the pressure becomes higher by $\Delta P^*=1.21$. Besides, the pressure dependence of Gibbs free energy is approximated by $\Delta G^*\approx V_m^*\Delta P^*$. The change in Gibbs free energy ΔG^* by ΔP^* is estimated as 1.2 when we use the molar volume as $V_m^*\approx1.0$.

In order to confirm what kind of transition takes place, the radial distribution functions (RDFs), which are shown in Fig. 5, were calculated at $T^*=0.835$, 1.04, and 1.25 for $P^*=3.63$ from the MuTh MC production run by the reweighting techniques. We observe four peaks at $r^*=1.10$, 1.60, 1.95, and 2.26 in the RDF at $T^*=0.835$, two peaks at $r^*=1.07$ and 1.97 in the RDF at $T^*=1.04$, and two peaks at $r^*=1.06$ and 2.01 in the RDF at $T^*=1.25$. The RDF at $T^*=0.835$ shows the characteristic curve of the solid state of face-centered-cubic crystal, and the RDF at $T^*=1.25$ shows that of liquid state, and the RDF at $T^*=1.04$ shows the intermediate curves between the two. Thus, we conclude that the first-order phase transi-

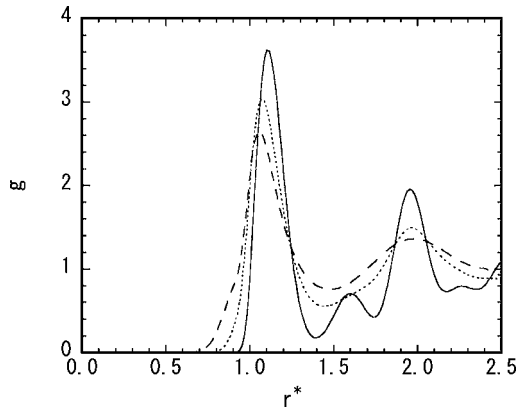

FIG. 5. The radial distribution functions at $T^*=0.835$, 1.04, and 1.25 for $P^*=3.63$ which is obtained from the MuTh MC production run by the reweighting techniques. The RDF at $T^*=0.835$ is shown by the solid line, at $T^*=1.25$ is shown by the dashed line, and at the transition temperature ($T^*=1.04$) is shown by the dotted line.

tion observed in the present simulation is the liquid-solid phase transition.

C. Reliability of thermodynamic quantities and probability distributions

The pressure $\langle P^* \rangle_{NPT}$, as well as the other thermodynamic properties discussed in the Sec. II B, was calculated from the MuTh MC production run by the reweighting techniques in Eq. (19). In Fig. 6, we compare the calculated pressure $\langle P^* \rangle_{NPT}$ with each given pressure P^* in the reweighting formula. In the temperature ranges from $T^*=1.17$ to 2.09 for $P^*=7.25$, from $T^*=1.11$ to 2.09 for $P^*=6.05$, from $T^*=0.695$ to 2.09 for $P^*=4.84$, from $T^*=0.723$ to 1.46 for $P^*=3.63$, and from $T^*=0.417$ to 1.01 for $P^*=2.42$, the difference between the calculated pressure $\langle P^* \rangle_{NPT}$ and the given

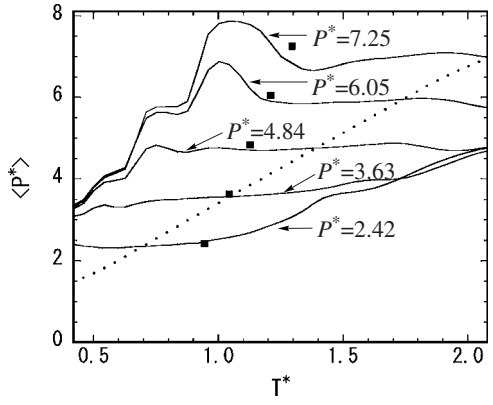

FIG. 6. Pressure as a function of temperature obtained from the MuTh MC production run. (a) Pressure as thermodynamic quantities, $\langle P^* \rangle_{NPT}$, that was calculated by the reweighting techniques for each given pressure in the reweighting formula of $P^*=2.42$, 3.63, 4.84, 6.05, and 7.25 are shown by solid lines, and (b) pressure $\langle P^* \rangle_{\text{therm}}$, which is calculated from Eq. (23), is shown by the dotted line. The expectation values were calculated at every $T^*=4.17 \times 10^{-2}$ from 0.417 to 2.09. Squares represent the transition points obtained from the simulation results for each pressure.

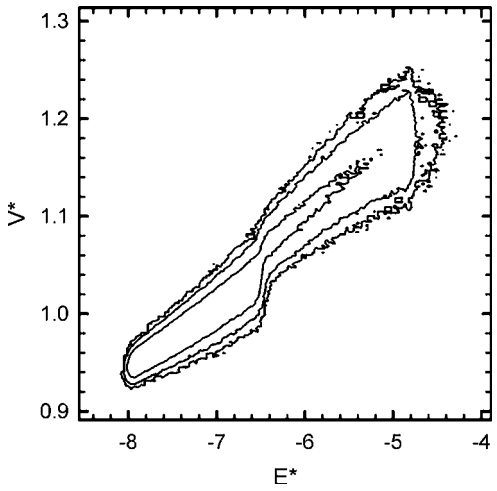

FIG. 7. The contour representation of the probability distribution $P_{\text{MuTh}}(E^*, V^*; P_0^*)$ in logarithmic scale that was obtained by the MuTh MC production run. The curves are the counter map of $\ln P_{\text{MuTh}}(E^*, V^*; P_0^*)=-8, -10$, and -12, and the outermost curve corresponds to -12.

pressure P^* in the reweighting formula is within 5%. The physical quantities for the given pressure P^* are considered to be reliable within these temperature ranges. The calculated pressure $\langle P^* \rangle_{NPT}$ slowly converged to $P^*=4.78$ at $T^*=2.09$ for the given pressure of $P^*=2.42$, 3.63 and 4.84, and gradually converged to $P^*=3.27$ at $T^*=0.417$ for the given pressure of $P^*=7.25$, 6.05, and 4.84. The physical quantities are less reliable for these regions. Therefore, we conclude that the stepwise changes in average volume, enthalpy, and entropy and the weak peaks in heat capacity below $T^*=1.00$ for $P^*=6.05$ and 7.25, which are shown in Figs. 4(a)–4(c) and 4(e), are not to have the same origin as the first-order phase transition, but are apart from the reliable temperature region.

Pressure $\langle P^* \rangle_{\text{therm}}$, which is calculated from Eq. (23), as a function of temperature is also shown in Fig. 6. We see that the pressure decays linearly from $(T^*, P^*)=(2.09, 6.97)$ to $(T^*, P^*)=(0.417, 1.49)$. The relation of $P^*=3.39T^*+0.0161$ is obtained by the least-squares fit, while the relation should be $P^*=3.47T^*$ from $P^*/T^*=P_0^*/T_0^*$ as $P_0^*=7.25$ and $T_0^*=2.09$ in the present simulation. This corroborates with the fact that the MuTh ensemble well samples the configurational space in the restricted pressure-temperature ratio $P^*/T^*=P_0^*/T_0^*$.

The contour map of the probability distribution $P_{\text{MuTh}}(E^*, V^*; P_0^*)$ obtained by the MuTh MC production run is shown in Fig. 7. The volume space does not spread over uniformly but slightly changes by keeping some volume size as the potential energy varies because the system is restricted by the initial pressure P_0 during the MuTh simulation. The remarkable change in the volume space is observed around the phase transition point. The changes in volume space are $\Delta V^*=0.11$ at $E^*=-6.5$ and $\Delta V^*=0.07$ at $E^*=-6.4$.

The contour maps of the probability distribution $P_{NPT}(E^*, V^*; T^*, P^*)$ are shown in Fig. 8. As the combination of (T^*, P^*) along $P^*/T^*=P_0^*/T_0^*$, we chose $(T^*, P^*)=(0.417, 1.45)$, $(T^*, P^*)=(1.04, 3.63)$, and $(T^*, P^*)=(2.09, 7.25)$. These distributions exactly coincide with the probability distribution $P_{\text{MuTh}}(E^*, V^*; P_0^*)$ in Fig. 7. This im-

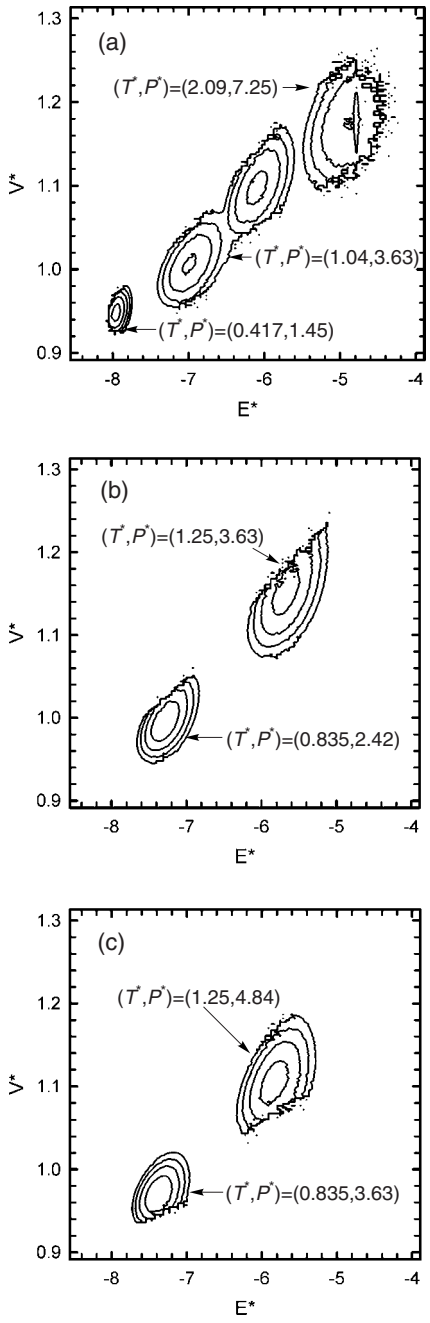

FIG. 8. The contour representation of the probability distributions $P_{NPT}(E^*,V^*;T^*,P^*)$ in logarithmic scale that was obtained from the MuTh MC production run by the reweighting techniques (a) along $P^*/T^*=P_0^*/T_0^*$, (b) below $P^*/T^*=P_0^*/T_0^*$, and (c) above $P^*/T^*=P_0^*/T_0^*$. The curves are the counter map of $\ln P_{NPT}(E^*,V^*;T^*,P^*)=-6,-8,-10$, and -12 and the outermost curve corresponds to -12 in each figure.

plies that the simulation well sampled from $(T^*,P^*)=(0.417,1.45)$ to $(T^*,P^*)=(2.09,7.25)$ along $P^*/T^*=P_0^*/T_0^*$. The probability distribution at $(T^*,P^*)=(1.04,3.63)$ is not only along $P^*/T^*=P_0^*/T_0^*$ but at the transition point. Therefore, we can observe two minima at $(E^*,V^*)=(-6.98,1.00)$ and at $(E^*,V^*)=(-6.10,1.10)$ and the saddle point at $(E^*,V^*)=(-6.54,1.05)$.

The probability distributions $P_{NPT}(E^*,V^*;T^*,P^*)$ apart from $P^*/T^*=P_0^*/T_0^*$ were also investigated. We chose a pair of $(T^*,P^*)=(0.835,2.42)$ and $(T^*,P^*)=(1.25,3.63)$ as the combination of (T^*,P^*) below $P^*/T^*=P_0^*/T_0^*$ and a pair of $(T^*,P^*)=(0.835,3.63)$ and $(T^*,P^*)=(1.25,4.84)$ as the combination of (T^*,P^*) above $P^*/T^*=P_0^*/T_0^*$. We observe each minimum at $(E^*,V^*)=(-7.28,1.00)$ for $(T^*,P^*)=(0.835,2.42)$ and $(E^*,V^*)=(-5.67,1.15)$ for $(T^*,P^*)=(1.25,3.63)$ and the left-top distribution is lacking in both distributions [see Fig. 8(b)]. Whereas we can observe each minimum at $(E^*,V^*)=(-7.40,0.970)$ for $(T^*,P^*)=(0.835,3.63)$ and $(E^*,V^*)=(-5.83,1.10)$ for $(T^*,P^*)=(1.25,4.84)$ and the right-bottom distribution is lacking in both distributions [see Fig. 8(c)]. This means that the probability distribution $P_{NPT}(E^*,V^*;T^*,P^*)$ shifts toward larger V^* for the combination of (T^*,P^*) below $P^*/T^*=P_0^*/T_0^*$ and toward smaller V^* for the combination of (T^*,P^*) above $P^*/T^*=P_0^*/T_0^*$. These probability distributions coincide with the probability distribution $P_{\mathrm{MuTh}}(E^*,V^*;P_0^*)$ in Fig. 7. The lack in the probability distributions originate from the configurational space sampled in the MuTh MC simulation. The choice of the combination of (T^*,P^*) far from $P^*/T^*=P_0^*/T_0^*$ leads to the serious lack in the probability distribution and also leads to unreliable physical quantities. Thus, the expectation values of the physical quantities are reliable for the configurational space along $P^*/T^*=P_0^*/T_0^*$, whereas the values are less reliable for the configurational space far apart from $P^*/T^*=P_0^*/T_0^*$.

IV. CONCLUDING REMARKS

In the present paper, we applied the MuTh MC method to the bulk Lennard-Jones fluid to investigate the liquid-solid phase transition. The phase transition between liquid and solid state was observed as the "discontinuity" of thermodynamic quantities. All the calculated phase transition temperatures were within the reliable temperature range for each given pressure, which is at P^*/T^* near P_0^*/T_0^*. The contour map of the probability distribution at temperature T and pressure P along $P^*/T^*=P_0^*/T_0^*$ gives ordinary population and that became waning as P^*/T^* apart from P_0^*/T_0^*. We can observe two distinct configurational spaces coexisting in the probability distribution at the phase transition point along $P^*/T^*=P_0^*/T_0^*$. The MuTh algorithm is a powerful simulation method to overcome the multiple-minima problem in the *N-P-T* ensemble and that is also applicable to the liquid-solid phase transition in the isobaric condition.

ACKNOWLEDGMENTS

The present work was supported, in part, by the Ministry of Education, Culture, Sports, Science and Technology of Japan (MEXT): One of the authors (C.M.) was supported by Grants-in-Aid for Young Scientists (B) Grant No. 16740244 and one of the authors (Y.O.) was supported by Grants-in-Aid for the Next Generation Super Computing Project, Nanoscience Program and for Scientific Research in Priority Areas, Water and Biomolecules.

[1] B. A. Berg and T. Neuhaus, Phys. Lett. B **267**, 249 (1991).
[2] B. A. Berg and T. Neuhaus, Phys. Rev. Lett. **68**, 9 (1992).
[3] B. A. Berg and T. Celik, Phys. Rev. Lett. **69**, 2292 (1992).
[4] U. H. E. Hansmann and Y. Okamoto, J. Comput. Chem. **14**, 1333 (1993).
[5] Y. Okamoto and U. H. E. Hansmann, J. Phys. Chem. **99**, 11276 (1995).
[6] W. Janke and S. Kappler, Phys. Rev. Lett. **74**, 212 (1995).
[7] N. B. Wilding, Phys. Rev. E **52**, 602 (1995).
[8] B. A. Berg and W. Janke, Phys. Rev. Lett. **80**, 4771 (1998).
[9] K. K. Bhattacharya and J. P. Sethna, Phys. Rev. E **57**, 2553 (1998).
[10] H. Liang and H. Chen, J. Chem. Phys. **113**, 4469 (2000).
[11] C. Muguruma, Y. Okamoto, and M. Mikami, Internet Electron. J. Mol. Des. **1**, 583 (2002).
[12] B. A. Berg, Comput. Phys. Commun. **147**, 52 (2002).
[13] E. Bittner, W. Janke, and D. B. Saakian, Phys. Rev. E **67**, 016105 (2003).
[14] B. A. Berg, Comput. Phys. Commun. **153**, 397 (2003).
[15] C. Muguruma, Y. Okamoto, and M. Mikami, J. Chem. Phys. **120**, 7557 (2004).
[16] C. Muguruma, Y. Okamoto, and M. Mikami, Croat. Chem. Acta **80**, 203 (2007).
[17] B. A. Berg, Fields Inst. Commun. **26**, 1 (2000).
[18] A. Mitsutake, Y. Sugita, and Y. Okamoto, Biopolymers **60**, 96 (2001).
[19] A. M. Ferrenberg and R. H. Swendsen, Phys. Rev. Lett. **61**, 2635 (1988); **63**, 1658 (1989).
[20] H. Okumura and Y. Okamoto, Phys. Rev. E **70**, 026702 (2004).
[21] H. Okumura and Y. Okamoto, Chem. Phys. Lett. **391**, 248 (2004).
[22] F. F. Abraham, Rep. Prog. Phys. **45**, 1113 (1982).
[23] S. Kirkpatrick, C. D. Gelatt, Jr., and M. P. Vecchi, Science **220**, 671 (1983).
[24] J. Solca, A. J. Dyson, G. Steinebrunner, B. Kirchner, and H. Huber, Chem. Phys. **224**, 253 (1997).
[25] A. Rytkönen, S. Valkealahti, and M. Manninen, J. Chem. Phys. **108**, 5826 (1998).
[26] M. A. van der Hoef, J. Chem. Phys. **113**, 8142 (2000).
[27] K. Maeda, W. Matsuoka, T. Fuse, K. Fukui, and S. Hirota, J. Mol. Liq. **102**, 1 (2003).
[28] L. Gómez, C. Gazza, H. Dacharry, L. Peñaranda, and A. Dobry, Phys. Rev. B **71**, 134106 (2005).
[29] V. G. Baidakov, S. P. Protsenko, and Z. R. Kozlova, Chem. Phys. Lett. **447**, 236 (2007).
[30] H. Okumura and F. Yonezawa, J. Non-Cryst. Solids **293–295**, 715 (2001).
[31] J. K. Brennan and W. Dong, Phys. Rev. E **67**, 031503 (2003).
[32] N. Metropolis, A. W. Rosenbluth, M. N. Rosenbluth, A. H. Teller, and E. Teller, J. Chem. Phys. **21**, 1087 (1953).
[33] B. A. Berg, Nucl. Phys. B, Proc. Suppl. **63A**, 982 (1998).
[34] A. M. Ferrenberg and R. H. Swendsen, Phys. Rev. Lett. **63**, 1195 (1989).
[35] S. Kumar, D. Bouzida, R. H. Swendsen, P. A. Kollmann, and J. M. Rosenberg, J. Comput. Chem. **13**, 1011 (1992).
[36] S. N. Chakraborty and C. Chakravarty, Phys. Rev. E **76**, 011201 (2007).
[37] P. Jena and W. R. Smith, Chem. Phys. Lett. **21**, 295 (1973).
[38] P. V. Giaquinta, G. Giunta, and S. Prestipino Giarritta, Phys. Rev. A **45**, R6966 (1992).
[39] J. U. Madsen and R. M. J. Cotterill, Phys. Lett. **83A**, 219 (1981).